

## Effect of High Temperature Heat Treatment on the Structure and Properties of FeCoCrNiZr Alloy

Jiasheng Shen (0000-0001-9022-4750)<sup>1</sup>, Sheng Lei (0000-0003-1764-6273)<sup>1,2\*</sup>, Jigen Fang (0000-0003-2163-2704)<sup>1</sup>, Yafeng Liu (0000-0002-4802-826X)<sup>1</sup>, Zhengqiang Hu (0000-0002-4419-720X)<sup>1</sup>, Shaojie Cui (0000-0002-5046-1089)<sup>1</sup>, Hailang Zhang (0000-0002-1618-6415)<sup>1</sup>, Zhengwei Xue (0000-0002-9160-8091)<sup>1</sup>

<sup>1</sup>School of Mechanical and Electrical Engineering, Anhui Jianzhu University, Hefei 230601, PR China.

<sup>2</sup>Key Laboratory of Intelligent Manufacturing of Construction Machinery, Hefei 230601, PR China. E-mail:[\\*leish1964@vip.126.com](mailto:leish1964@vip.126.com)

FeCoCrNiZr high-entropy alloy was melted by vacuum arc melting. The alloys were vacuum annealed at 873, 1073, and 1273 K, respectively. The microstructure, compressive mechanical properties, thermal stability, and hardness of as-cast and annealed FeCoCrNiZr alloys at different annealing temperatures were investigated by using X-ray diffractometry (XRD), scanning electron microscopy (SEM), microhardness tester and universal material testing machine. The results reveal that it has no noticeable change in the phase composition of the alloy after high temperature annealing. The as-cast FeCoCrNiZr alloy is composed of the body-centred cubic phase and Laves phase. In the 1073 K annealed state, the  $\sigma$ -phase was detected in the alloy, and the alloy's hardness reached a maximum value of 915.94 HV<sub>0.2</sub>. The hardness of the alloy in the annealed state is obviously higher than that of the as-cast alloy, and the increased compressive strength is the result of the combined effect of the hardening of the C15 Laves phase and the solid solution strengthening of the Zr atoms.

**Keywords:** High-entropy alloy, Annealing, Microstructure, Compressive properties, Microhardness

### 1 Introduction

High-entropy alloys (HEAs), compared with other alloys are more stable at high temperature as well as more resistant to high temperature oxidation. Compared to single-phase HEAs, multi-phase HEAs exhibit higher yield strength and better high temperature properties. HEAs are known for their large atomic disorder, which will be greater at high temperatures, so HEAs become more stable in both crystalline and amorphous states. It bears a solid solution-strengthening effect, allowing for very high temperature strength [1-4]. A review of the existing literature on HEAs shows that the FeCoCrNi-based HEA alloy is one of the extensively studied HEAs. The high-entropy alloy system not only presents a simple microstructure but also has excellent overall performance and heat treatment has a positive effect on improving alloy properties [5-7]. The FeCoCrNi-based HEA alloy exhibits a single face-centred cubic solid solution with superior mechanical properties. The study of the high temperature properties of FeCoCrNi-based HEA alloy is of great significance for scientific research and industrial applications [8, 9].

C15 Laves phase is a gas-absorbing element having the ability to collect free gases (e.g. hydrogen) and can be used in nuclear applications. The CoCrFeNiZr<sub>x</sub> alloy consists of a body-centred cubic solid solution and the laves phase. The typical sub-eutectic microstructure was identified in the as-cast alloy

having  $x=0.1\sim0.4$ , while the typical eutectic microstructure was identified in the as-cast alloy having  $x=0.5$ . For sub-eutectic CoCrFeNiZr<sub>x</sub>, the volume fraction of eutectic microstructure increases with the increasing  $x$  content. The resulting eutectic alloy consists of a face-centred cubic solid solution and alternating layers of Laves phase. The structure of sub-eutectic alloys consists of face-centred cubic primary crystalline solid solutions and eutectic clusters. An increase in Zr content leads to not only an increase in the volume fraction of the laves phase and alloy strength but also in brittleness [10, 11].

However, there are few research results on the correlation between the properties and composition of FeCoCrNi alloys with Zr addition by heat treatment, and some scholars have only focused on studying the effect of annealing temperature on the phase of FeCoCrNiZr alloy or on the effects of annealing on the properties of the alloy. For these reasons, FeCoCrNiZr alloy was prepared by vacuum arc smelting in this paper to study the microstructural evolution process, phase structure, and high temperature stability of FeCoCrNiZr alloy under different annealing temperatures [12, 13].

### 2 Experimental

Fe, Co, Cr, Ni, and Zr (purity >99.9 wt.%) were smelted by vacuum arc melting. The arc-melted ingots are repeated and remelted at least five times to ensure

a homogeneous composition. After natural cooling, a cylindrical sample with a diameter of 5 mm and a length of 10 mm is cut by wire cutting. The samples were vacuum annealed at 873, 1073, and 1273 K for 2 hours. The cast and annealed alloys were polished to a mirror finish using a grinder (EcoMet 30), the metallographic specimens were etched with aqua regia ( $\text{HCl:HNO}_3 = 3:1$ ) for 10s, and the surface morphology of the samples was observed using a scanning electron microscope (Hitachi s-4800). The phase composition of the cast and annealed alloys were examined using an X-ray diffractometer (X'Pert Pro MPD). The hardness of the alloy was determined using a microhardness tester (Wolpert Wilson 401MVD). Five testing points were selected on the

surface of the specimen, and each measurement point was spaced at 200  $\mu\text{m}$  intervals with a load of 0.2 kg and a holding time of 15 s. During this process, the average hardness value was calculated. The thermal stability of the HEAs was studied using a simultaneous thermal analyser (TGA-DSC), heated to 1273 K at a rate of 20 K/min and protected by nitrogen gas, and cooled to ambient temperature with the furnace. A universal testing machine (Instron MTS Sans) was used to test the compressive properties of the specimens at room temperature with a compressive strain rate of  $10^{-3} \text{ S}^{-1}$ . The composition of the FeCoCrNiZr high entropy alloy is shown in Tab. 1. Tab. 2 illustrates the atomic radii and binary mixing enthalpies of the elements.

**Tab. 1** The composition of FeCoCrNiZr high-entropy alloy

Elements	Fe	Co	Cr	Ni	Zr
at.%	20	20	20	20	20
wt.%	17.64	18.64	16.43	18.54	28.75

**Tab. 2** Binary mixing enthalpies (in  $\text{kJ/mol}$ ) and atomic sizes of different elements

Atomic radius/pm	Co	Cr	Fe	Ni	Zr
Co(126pm)	-	-4	-1	0	-41
Cr(127pm)	-4	-	-1	-7	-12
Fe(127pm)	-1	-1	-	-2	-25
Ni(124pm)	0	-7	-2	-	-49
Zr(160pm)	-41	-12	-25	-49	-

### 3 Results and discussion

#### 3.1 XRD analysis

Figure 1 illustrates the XRD patterns of FeCoCrNiZr alloy in the as-cast state and at different annealing temperatures. The main phases are the BCC phase and the C15 Laves phase and they are unchanged and constant under different annealing conditions. However, a new minor phase  $\sigma$ -phase was detected at an annealing temperature of 1073 K. As the four basic elements, Fe, Co, Cr, and Ni, are present in the compound in similar concentrations and are frequently interchangeable in the CoCrFeNiZr alloy, the composition of the compound is considered to be  $(\text{Cr}, \text{Fe}, \text{Co}, \text{Ni})_{77.6}\text{Zr}_{22.4}$ , or  $(\text{Cr}, \text{Fe}, \text{Co}, \text{Ni})_3\text{Zr}$ . As the annealing temperature increases, the relative intensity of the Laves phase increases as well, indicating that the volume fraction of the precipitated phase is increasing and becoming the dominant phase, which reveals that the FeCoCrNiZr alloy is in the nature of excellent thermal stability [14]. The phase transformation at different annealing temperatures is due to the presence of sub-stable supersaturated solid solution phases, which evolve into stable phases in the final stage of annealing [15]. The increased intensity of the

XRD peaks is also associated with the coarser dendrite morphology formed during the annealing process. Therefore, the possible solidification path for FeCoCrNiZr alloy is,  $\text{L} \rightarrow \text{L}1 + \text{C}15$  Laves phase  $\rightarrow$  eutectic (BCC + C15 Laves phase) + C15 Laves phase.

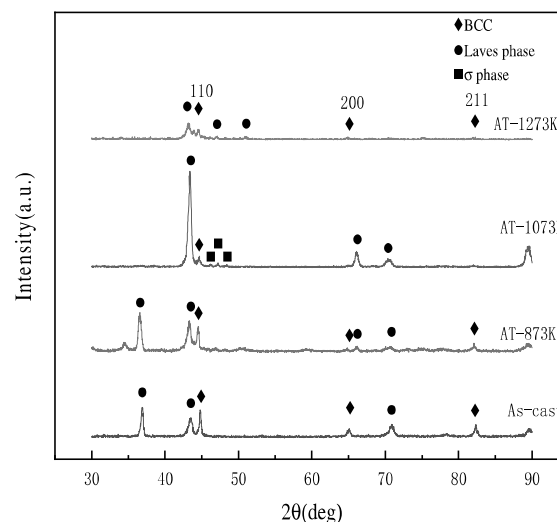


**Fig. 1** XRD patterns of FeCoCrNiZr alloys in the as-cast state and at different annealing temperatures

### 3.2 Microstructure analysis

As illustrated in Figure 2, the microstructure of the FeCoCrNiZr alloy is presented at different annealing temperatures. The dendrites are C15 Laves phase, while the interdendritic region forms a eutectic structure consisting of a body-centred cubic phase (charcoal grey) and a C15 Laves phase (french grey). Regardless of the annealing conditions, a dendritic structure similar to the cast alloy is observed. In the 1073K annealed alloy, the FeCoCrNiZr alloy was detected by XRD to contain the presence of the  $\sigma$ -phase. As illustrated in Figure 2d, the  $\sigma$ -phase coexists with the body-centred cubic phase in the interdendritic region, and the formation of a small number of new phases is observed either between or near the dendrites [16]. As illustrated in Table 3, the

dendrites and interdendritic of the FeCoCrNiZr alloy were spots scanned by EDS and found to be rich in Co, Ni, and Zr elements in the dendrites and Fe and Cr elements in the interdendrites [17]. With the increase of annealing temperature, the Cr element gradually deviates to the dendrites, and the content increases from 46.28 mol.% to 52.99 mol%. The Ni element diffuses and deviates towards the dendrites, and though the Ni element content between the dendrites gradually decreases, the Ni content in the dendrites increases from 21.10 mol.% to 24.12 mol%. The Fe, Co, and Zr elements do not vary much during the annealing process at different temperatures, but at 1073K annealing temperature, the interdendritic Zr element content is elevated due to the precipitation of a  $\sigma$ -phase with an atomic ratio of ZrFe<sub>3</sub> between the dendrites.

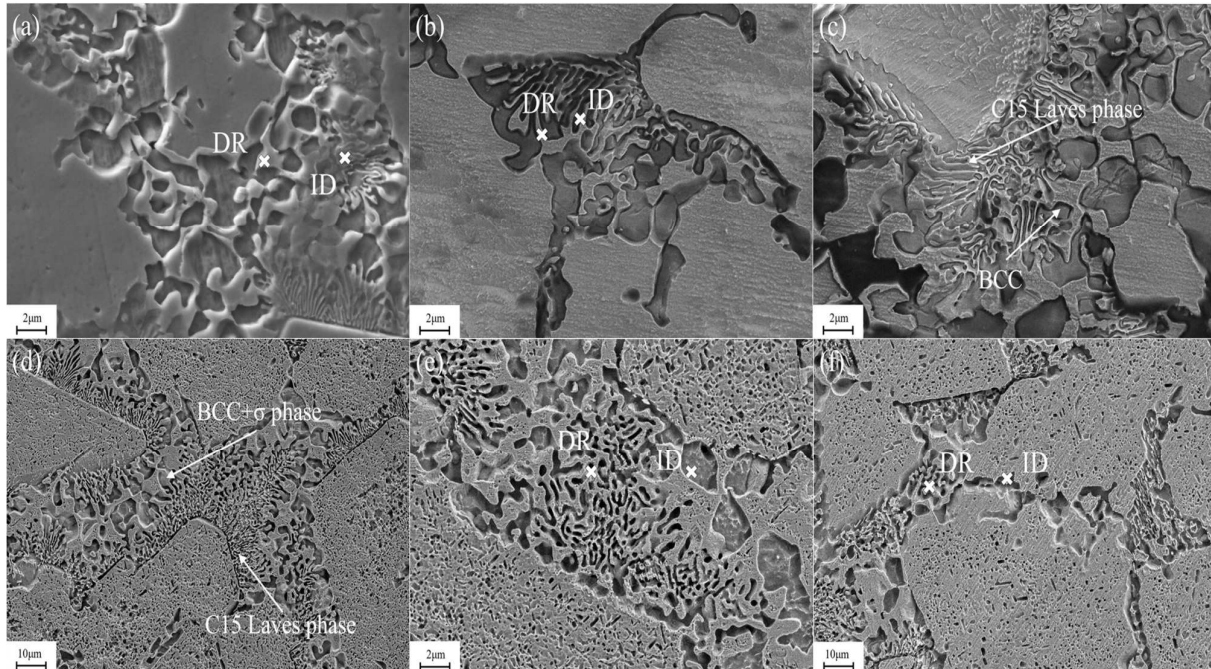


**Fig. 2** SEM images of FeCoCrNiZr alloys in an as-cast state and at different annealing temperatures: (a) As-cast; (b, c) AT-873 K; (d, e) AT-1073 K; (f) AT-1273 K

**Tab. 3** Composition distribution of micro-regions in FeCoCrNiZr alloys in the as-cast state and at different annealing temperatures

State	Position	Mole fraction/%				
		Cr	Fe	Co	Ni	Zr
As-cast	DR	13.67	17.89	22.41	21.10	24.93
	ID	46.28	28.07	12.60	10.81	2.24
AT-873K	DR	10.85	18.23	24.22	23.09	23.61
	ID	47.76	27.24	13.67	8.38	2.95
AT-1073K	DR	9.87	18.86	22.52	23.56	25.19
	ID	48.90	28.71	10.23	6.79	5.37
AT-1273K	DR	8.56	18.81	23.76	24.12	24.75
	ID	52.99	28.25	10.13	6.28	2.35

### 3.3 Thermal analysis

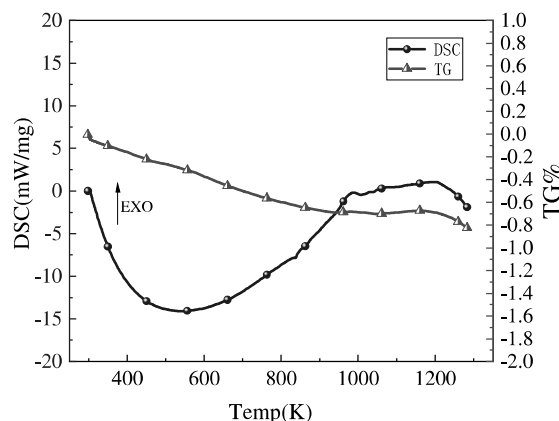


**Fig. 3** TG-DSC curves of FeCoCrNiZr alloys

Figure 3 illustrates the results of the TG-DSC curves for the FeCoCrNiZr alloy during heating from room temperature to 1273 K [18]. At higher temperatures, changes in thermogravimetric behavior are usually evident, but in this experiment, the thermogravimetric curve showed a maximum weight loss of 0.816 tg.%, which is attributed to the decomposition of trace surface oxides and the trace amorphous crystallization [19,20]. Remarkably, there is no significant change in mass, which indicates the commendable thermal stability of the FeCoCrNiZr alloy in the temperature range from room temperature to 1273 K. The DSC curve shows a downward trend below 523 K, which is caused by the gradual destruction of the crystal structure caused by the increasing temperature. The long DSC exothermic lines from 523 K to 973 K are associated with the release of internal stresses, such as the release of solid solution

lattice distortion energy. The exothermic peak above 973 K is associated with the release of energy during the phase transformation [21]. Whether the FeCoCrNiZr alloy undergoes a phase transformation in the temperature field can be determined by the exothermic and endothermic peaks on the DSC curve. The DSC curve is no obvious exothermic or endothermic peak, which is probably due to the intermetallic compounds in the FeCoCrNiZr alloy releasing or absorbing little heat during the phase transformation in the whole temperature range, indicating that the FeCoCrNiZr alloy has excellent thermal stability [22].

### 3.4 Microhardness analysis

The microhardness values of the FeCoCrNiZr alloy in the as-cast state and at different annealing temperatures were averaged by taking five measurements at 0.2 mm intervals, as illustrated in Table 4. The microhardness of the alloy at annealing temperatures of 873, 1073, and 1273 K are all increased compared to the as-cast alloy. The microhardness of the FeCoCrNiZr alloy reaches a maximum value of 915.94 HV<sub>0.2</sub> at an annealing temperature of 1073 K. At this point, the alloy consists of the body-centred cubic phase, the C15 Laves phase and the  $\sigma$ -phase. Since the  $\sigma$ -phase is a complex intermetallic compound, the presence of the  $\sigma$ -phase contributes more to the microhardness of the alloy than the body-centred cubic. At an annealing temperature of 1073 K, the intensity of the C15 Laves phase peak is much higher than that of the body-centred cubic phase peak, indicating that the Laves phase accounts for a more significant volume fraction of the main phase of the alloy and is more resistant to temper softening.

**Tab. 4** Microhardness values of FeCoCrNiZr alloys in the as-cast state and at different annealing temperatures (HV<sub>0.2</sub>)

State	As-cast	AT-873K	AT-1073K	AT-1273K
1	502.5	776.1	910.6	834.6
2	531.2	835.0	939.5	893.1
3	538.1	796.4	889.5	870.2
4	498.2	789.8	943.4	864.7
5	511.5	812.3	896.7	886.8
average	516.30	801.92	915.94	869.88

### 3.5 Compression mechanical property analysis

Figure 4 illustrates the stress-strain curves for the FeCoCrNiZr alloy in the as-cast state and at different annealing temperatures, and the values for the compressive properties are illustrated in Table 5. With the increase in annealing temperature, the microhardness of the FeCoCrNiZr alloy reached a maximum value of 915.94 HV<sub>0.2</sub> at 1073 K annealing

temperature, and the compressive strength of the alloy increased from 531.2 MPa to 1164.2 MPa. The plasticity of the FeCoCrNiZr alloy in different states does not change much in general, and the brittle hardness is more considerable. The physical phase diffraction peak intensity of the alloy after annealing at 873 K is not very different from that of the as-cast alloy, but the compressive strength has increased by

286.1 MPa. More defects arise due to the preferential nucleation at vacancies and other point defects in the solid state phase transition of cast multi-principal alloys [23, 24]. After annealing at 1073 K, the  $\sigma$ -phase in the alloy increases, improving the corresponding solid solution strengthening of the matrix and slightly increasing the strength of the alloy compared to that after annealing at 873 K. As can be seen from the XRD pattern, the diffraction peak intensity of the C15 Laves phase decreases significantly after annealing at 1273 K, indicating a decrease in the volume fraction. Since the presence of the Laves phase is the crucial reason for the greater brittleness of the FeCoCrNiZr alloy, the compressive strength of the annealed alloy is significantly increased. The compressive strength results from a combination of the hardening of the C15 Laves phase and the solid solution strengthening of the Zr atoms.

**Tab. 5** Room temperature compression performance parameters of as-cast and annealed FeCoCrNiZr alloys

State	$\sigma_y$ (MPa)	$\sigma_f$ (MPa)	$\varepsilon_f$ (%)
As-cast	273.3	531.2	3.3
AT-873K	776	817.3	3.9
AT-1073K	641	896.6	3.7
AT-1273K	530	1164.2	4.1

### 3.6 Fracture Morphology Analysis

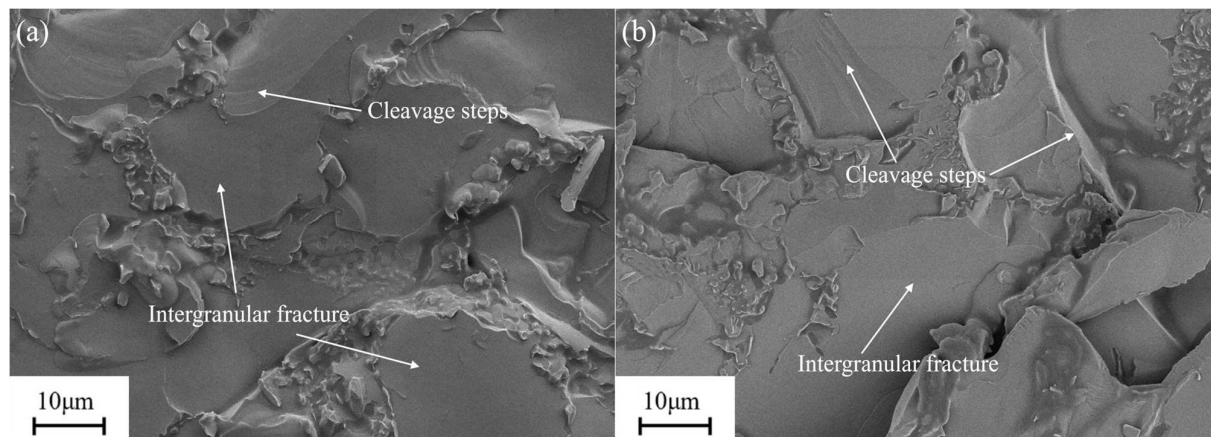


**Fig. 5** SEM image of the compression fracture of FeCoCrNiZr alloys

Figure 5 illustrates the main characteristic of fracture in FeCoCrNiZr alloys is endowed with a relatively smooth surface, and slight plastic deformation, which means that the ductility of FeCoCrNi alloys is reduced after the addition of Zr, and the fracture mechanisms are brittle fracture and cleavage fracture. Microcracking was observed in the Laves phase flakes, which implies increased brittleness of the alloy, consisting of the observed stress-strain curve [25-27]. The addition of equimolar ratios of Zr elements makes the volume fraction of the Laves phase comparable to that of the matrix body-centred cubic phase, the deformability of the C15 Laves phase

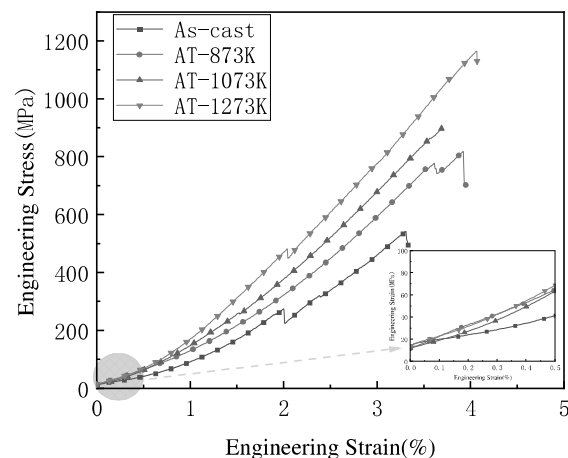


**Fig. 4** Compressive stress-strain curves of FeCoCrNiZr alloys in cast state and at different annealing temperatures

is limited and affected by microcracking under the action of strain, and the large volume mass fraction of the Laves phase inevitably makes the alloy hard and friable at room temperature [28, 29]. The alloys under stress cause grain-piercing fractures due to the low solid solution of Zr elements in the body-centred cubic phase. Owing to the inevitable presence of some segregation, precipitation, etc., in the alloy, the disconnection of the deconstruction is a rough crystal surface and showed a step type, and a more significant number of tearing ribs will retard the expansion of the crack [30].

## 4 Conclusions

- The ductility of FeCoCrNi alloy decreases after the addition of Zr. The fracture mechanism is a brittle fracture along with the crystal and deconvolution fracture, and the brittleness of the alloy increases.
- The FeCoCrNiZr alloy shows a new minor phase  $\sigma$ -phase after annealing at 1073 K. At this moment, the alloy consists of the body-centred cubic phase, the C15 Laves phase, and the  $\sigma$ -phase. As the  $\sigma$ -phase is a complex intermetallic compound, the presence of the  $\sigma$ -phase increases the microhardness of the alloy. The microhardness of the FeCoCrNiZr alloy reaches a maximum value of 915.94 HV0.2 at an annealing temperature of 1073 K. The phase composition does not change significantly with different annealing temperature conditions.
- As the annealing temperature increases to 1273 K, the compressive strength of the alloy increases from 531.2 MPa to 1164.2 MPa. The plasticity of the FeCoCrNiZr alloy in the annealed state did not change much at different temperatures, and the brittle hardness was more significant at this moment. The increase in compressive strength results from the combination of the hardening of the C15 Laves phase and solid solution strengthening of the Zr atoms.

## Acknowledgement

*This work has been supported by the Natural Science Foundation of the Higher Education Institutions of Anhui Province under Grant No. KJ2020ZD42.*

## References

- [1] ANCHEN, F.; JIANHONG, L.; MINGHUNG, T., On the phase constituents of four CoCrFeNiX ( $X=Y, Ti, Zr, Hf$ ) high-entropy alloys after prolonged annealing. *Journal of Materials Research and Technology* 2020, 9 (5), 11231-11243.
- [2] XUEHUI, Y.; YONG, Z., Functional properties and promising applications of high entropy alloys. *Scripta Materialia* 2020, 187, 188-193.
- [3] YE, Y.F.; WANG, Q.; LU, J.; LIU, C.T.; Yang, Y., High-entropy alloy: challenges and prospects. *Materials Today* 2016, 19 (6), 349-362.
- [4] XIAOHUA, C.; WEIYANG, X.; JIN, Z.; ZIDONG, W.; YANLIN, W.; YIFEI, M.; MING, Y.; WENWEN, J.; HUIWEN, Y.; YIDONG, W.; XIDONG, H., Influences of Ti additions on the microstructure and tensile properties of AlCoCrFeNi<sub>2.1</sub> eutectic high entropy alloy. *Intermetallics* 2021, 128, 107024.
- [5] HONGBO, X.; GUIZHONG, L.; JINGJIE, G., Effect of Mn, V, Mo, Ti, Zr elements on the organization and high temperature oxidation properties of AlFeCrCoCu-X high entropy alloy. *The Chinese Journal of Nonferrous Metals* 2015, 25(01), 103-110.
- [6] HANA, T.; FILIP, P., Partial Substitution of Mn by Al in the CoCrFeNiMn<sub>x</sub>Al<sub>20-X</sub> ( $X=5, 10, 15$ ) High Entropy Alloy Prepared of Mechanical Alloying and Spark Plasma Sintering. *Manufacturing Technology* 2022, 22(3), 342-346, DOI: 10.21062/mft.2022.045.
- [7] DAVID, B.; ANTONÍN, K.; JAN, N.; ZBYNĚK, S., The Effect of Boriding and Heat Treatment on the Structure and Properties of 100Cr6 Steel. *Manufacturing Technology* 2022, 22(1), 2-9, DOI: 10.21062/mft.2022.003.
- [8] YUE, J.; GUANGTAI, Z.; SIMENG, C.; X.M. Li., Organization and properties of CrFeCoNiTi<sub>1-x</sub> high-entropy alloys, *J. Journal of Harbin University of Science and Technology* 2020, 25 (06), 112-118.
- [9] JUNLUN Z.; XIANLUN, Y.; DONG, Y.; YIPING, L.; JIANG, L.; WANG, T.M.; LI, T.J., Corrosion properties of Al<sub>x</sub>CoCrFeNiTi<sub>0.5</sub> high entropy alloys in 0 • 5M H<sub>2</sub>SO<sub>4</sub> aqueous solution. *Materials Research Innovations* 2014, 18 (sup4), 756.
- [10] WENNA, J.; HUI, J.; DONGXU, Q.; JUNYANG, H.; HONGLIANG, Z.; YIPING, L.; TINGJU, L., Effects of Mo on microstructure and mechanical properties of Fe<sub>2</sub>Ni<sub>2</sub>CrMox eutectic high entropy alloys. *Materials Chemistry and Physics* 2021, 260, 24175.
- [11] WENYI, H.; HUI, Z.; FANG, F.; ZONGHAN, X.; JIANQING, J., Microstructure and mechanical properties of CoCrFeNiZrx eutectic high-entropy alloys. *Materials & Design* 2017, 134, 226-233.
- [12] LUDMILA, K.; LVETA, T.; ADAM, S., Effect of various heat and thermo-mechanical treatments on low alloyed CMnAlNb high strength steel. *Manufacturing Technology* 2021, 21(6), 824-828, DOI: 10.21062/mft.2021.094.

- [13] MICHAL, P.; HANA, J.; KATEŘINA, R.; TOMÁŠ, J.; RADOVAN, B., Microstructural Evolution in 42SiCr Steel in a High-Temperature Chamber Under Microscope Objective. *Manufacturing Technology* 2020, 20(3), 355-360, DOI: 10.21062/mft.2020.053.
- [14] W.H, L.; Z.P, L.; J.Y, H.; J.H, L.; Z.J, W.; B, L.; Y, L.; M.W, C., Ductile CoCrFeNiMox high entropy alloys strengthened by hard intermetallic phases. *Acta Materialia* 2017, 134, 226-233.
- [15] YUFANG, Z.; JINYU, Z.; YAQIANG, W.; SHENGHUA, W.; XIAOQING, L.; KAI, Wu.; GANG, L.; JUN, S., The metastable constituent effects on size-dependent deformation behavior of nanolaminated micropillars: Cu/FeCoCrNi vs Cu/CuZr. *Journal of Materials Science & Technology* 2021, 68 (09), 16-29.
- [16] VRTNIK, S.; GUO, S.; SHEIKH, S.; JELEN, A.; KOŽELJ, P.; LUZAR, J.; KOCJAN, A.; JAGLIČIĆ, Z.; MEDEN, A.; GUIM, H.; KIM, H.J.; DOLIN Š EK, J., Magnetism of CoCrFeNiZr<sub>x</sub> eutectic high-entropy alloys. *Intermetallics* 2018, 93, 122-133.
- [17] XI, B.; WEI, F.; JIWEI, L.; RUOBIN, C.; HANYANG, YU.; JIAOHUI, YAN.; XIN, Z.; FUXING, Y., Effect of Cr content on precipitation behavior of (CoCrNi)94Ti3Al3 medium entropy alloys. *Intermetallics* 2021, 132, 107125.
- [18] ZHENG, Z.; ZHONGKA, Y.; HAO, C.; WEIHUAO, L., Effect of Al Content on Microstructure and Nanoindentation Creep Behaviors of AlxFeCoNiCu High-entropy Alloys. *Hot Working Technology* 2019, 48, 62-65.
- [19] LIMING, S.; YI, X., Amorphous behavior of ZrxFeNiSi0.4B0.6 high entropy alloys synthesized by mechanical alloying. *Journal of Non-Crystalline Solids* 2020, 530, 119854.
- [20] MICHAEL, M.; GERALD, R.; JIRI, S., The Effect of Cryogenic Mechanical Alloying and Milling Duration on Powder Particles' Microstructure of an Oxide Dispersion Strengthened FeCrMnNiCo High-Entropy Alloy. *Metallurgical and Materials Transactions A* 2021, 53, 1-12.
- [21] SHENG, L.; ZHENGWEI, X.; YAFENG, L.; YUN, L.; DONGSHENG, J.; PING, W., Effect of annealing temperature on the structure and properties of FeCoCrNiMo high-entropy alloy. *High Temperature Materials and Processes* 2022, 41, 417-423.
- [22] LIMING, S.; YI, X., Amorphous behavior of ZrxFeNiSi0.4B0.6 high entropy alloys synthesized by mechanical alloying. *Journal of Non-Crystalline Solids* 2020, 530, 119854.
- [23] QINGXUAN, S.; ZHEN, W.; JIANG, W.; SHURONG, X.; BO, L.; QUAN, Y.; FENGJUN, Z.; LE, G.; JUN, L., Additive manufacturing of CoCrFeNiMo eutectic high entropy alloy: microstructure and mechanical properties. *Journal of Alloys and Compounds* 2022, 913, 165239.
- [24] B.X, C.; T, Y.; L, F.; J.H, L.; Z.B, J.; C.T, L., Refractory alloying additions on the thermal stability and mechanical properties of high-entropy alloys. *Materials Science and Engineering A* 2020, 797, 140020.
- [25] GANG, Q.; RUIRUN, C.; HUITING, Z.; HONGZE, F.; LIANG, W.; YANGQING, S.; JINGJIE, G.; HENGZHI, F., Strengthening FCC-CoCrFeMnNi high entropy alloys by Mo addition. *Journal of Materials Science & Technology* 2019, 35 (4), 578-583.
- [26] MOON, J.; TABACHNIKOVA, E.; SHUMILIN, S.; HRYHOROVA, T.; ESTRIN, Y.; BRECHTL, J.; PETER K, L.; WENQING, W.; KARIN A, D.; ZARGARAN, A.; JAEWUNG, B.; HYEON-SEOK, D.; BYEONG-JOO, L.; KYOUNGSEOP, K., Deformation behavior of a Co-Cr-Fe-Ni-Mo medium entropy alloy at extremely low temperatures. *Materials Today* 2021, 50, 55-68.
- [27] ECKER, J.; HE, G.; ZHEFENG, Z.; LÖSER, W., Fracture-induced melting in glassy and nanostructured composite materials. *Metastable Nanocrystal Mater* 2004, 20-21, 357-365.
- [28] BELKHOUANE, S.; BENTOUAF, A.; RACHED, H.; BOUYAKOUB ZAHIRA, A., Electronic structure, magnetic and structural properties of binary cubic C15 Laves phases PrX<sub>2</sub> (X = Co and Fe): a first-principles study. *Applied Physics A*, 2021, 127 (11), 835.
- [29] MENGDI, Z.; LIJUN, Z.; JIANTAO, F.; PENGFEI, Y.; GONG, L., Novel Co-free CrFeNiNb0.1Tix high-entropy alloys with ultra high hardness and strength. *Materials Science & Engineering A* 2019, 764 (C), 138212.
- [30] JIALE, M.; BAOLIN, W.; GUOSHENG, D.; LU Z.; GANG, W.; LI, Z.; NAIFU, Z.; YANDONG, L., The synergistic addition of Al, Ti, Mo and W to strengthen the equimolar CoCrFeNi high-entropy alloy via thermal-mechanical processing. *Journal of Alloys and Compounds* 2022, 911, 902.